Early growth response (Egr)-1: A novel anti-fibrotic mediator in liver

By

Briana Holt

Submitted to the graduate degree program in Toxicology and the Graduate Faculty of the University of Kansas in partial fulfillment of the requirement for the degree of Master of Science.

Chairperson Michele Pritchard, PhD

Bruno Hagenbuch, PhD

John Wood, PhD

Date Defended: 12/1/2014

The Thesis Committee for Briana Holt certifies that this is the appropriate version of the following thesis:

Early growth response (Egr)-1: A novel anti-fibrotic mediator in liver

Chairperson Michele Pritchard, PhD

Date approved: 12/5/2014

Abstract

Chronic alcohol consumption can lead to an aberrant wound healing response of the liver, or hepatic fibrosis. Egr-1 is an essential regulator of many genes involved in the orchestration of tissue injury and repair, yet the implications of Egr-1 in different models of liver disease remain unclear. Previously, we demonstrated that carbon tetrachloride (CCl_4)-induced hepatic fibrosis is enhanced in Egr-1 deficient mice. In this study, we investigated the role of Egr-1 in the attenuation of early markers of hepatic fibrosis using a model of ethanol-accelerated, CCl_4-induced liver injury in wild-type and Egr-1 deficient mice. Whereas *Egr-1* mRNA was induced 100-fold in livers from wild-type mice 48h after CCl_4 exposure, ethanol feeding reduced *Egr-1* expression by 50 percent. Seventy-two hours after CCl_4 exposure, hepatic mRNA accumulation of type I collagen and αSMA, markers of fibrogenesis expressed by activated hepatic stellate cells (HSC), were increased 22-fold and 20-fold, respectively, in both wild-type and *Egr-1 -/-* mice; levels of these transcripts were greater in ethanol-fed, *Egr-1 -/-* mice. Consistently, plate-induced activation of HSC from Egr-1 deficient mice was increased relative to HSC from wild-type mice. Previous use of an oxidant stress, antioxidant defense pathway array identified genes differentially expressed in ethanol-fed, *Egr-1 -/-* mice compared to ethanol-fed, wild-type mice after CCl_4 exposure. We examined one of these genes, NAD(P)H dehydrogenase, quinone 1 (Nqo1), and found that Nqo1 mRNA and protein was reduced in *Egr-1 -/-* mice relative to wild-type mice 72h after CCl_4 exposure, and ethanol feeding exacerbated this reduction. Consistently, chromatin from livers of wild-type, CCl_4-treated mice confirmed association between Egr-1 and the *Nqo1* promoter upon immunoprecipitation with an Egr-1 antibody. Although Egr-1 deficient mice did not

demonstrate inhibited oxidation of NADH after CCl_4 via loss of Nqo1, β-lapachone-mediated stimulation of Nqo1 activity suppressed CCl_4-induced liver injury and fibrogenic changes. Collectively, these data support the hypothesis that Egr-1 attenuates early markers of hepatic fibrosis, and here we propose that Nqo1, a previously unrecognized target of Egr-1, is a contributing factor.

Acknowledgements

I would like to acknowledge the help and support of my mentor, Michele Pritchard, throughout the course of my thesis research. I would also like to acknowledge my committee members for the ideas, suggestions, and words of encouragement during this process. Thanks to my family and friends for the moral support and acceptance of my decisions; and finally, I'd like to acknowledge the sources that funded this research: B.R.H (T32 ES007079-26A2) and M.T.P (P20 GM103549, R00 AA017918).

Table of Contents

Introduction

Consequences of alcohol consumption remain a financial burden on United States healthcare. In 2006, an estimated 220 billion dollars in economic costs were spent due to excessive alcohol consumption [1]. Alcoholic liver disease (ALD), which includes a spectrum of liver pathologies ranging from fatty liver, or steatosis, to steatohepatitis, fibrosis, and cirrhosis, accounts for 1 in 10 deaths in adults aged 20-64 years and is increasing in prevalence [2]. While early stages of ALD can regress with abstinence from alcohol, cirrhosis, or end stage liver disease, can only be cured by liver transplantation. In an effort to discover earlier interventions and potential therapeutic targets, much research has been done to investigate the mechanisms of alcohol toxicity in the early stages of liver disease progression.

Through a number of different mechanisms, alcohol acts to stimulate the build-up of triglycerides in the liver. Alcohol metabolism commonly occurs by the oxidation of ethanol to acetaldehyde and acetic acid by alcohol dehydrogenase (ADH) and acetaldehyde dehydrogenase (ALDH), respectively [3]. Under normal conditions, the balance between the oxidized and reduced form of nicotinamide adenine dinucleotide (NAD) is in favor of NAD+, the oxidized state; however, during ethanol metabolism increased levels of NADH accumulate intracellularly as NAD is reduced in both reactions [3]. The accumulation of NADH, an essential electron donor for many metabolic processes, stimulates the accumulation of free fatty acids (FA) through induction of FA synthesis and the simultaneous inhibition of β-oxidation and peroxisome proliferator-activated receptor- α (PPARα) [4]. This ethanol-induced hyperlipidemia leads to hepatic steatosis, the essential first step in liver disease progression.

While only 15-20% of patients with steatosis progress to fibrosis and cirrhosis [5], fatty liver increases susceptibility to the fibrogenic wound healing response and other advanced stages of liver disease. Through numerous pathways, FA accumulation can trigger the activation of hepatic stellate cells (HSC) to enhance their proliferation and extracellular matrix production and secretion—a hallmark of fibrosis. It is thought that in addition to ethanol, fatty acids upregulate the expression of CYP2E1, and CYP2E1-induced production of reactive oxygen species (ROS) leads to peroxidation of these fatty acids and mitochondrial damage [3]. This lipid peroxidation can then stimulate collagen synthesis and promote inflammation. Fatty liver has also been associated with increased periportal fibrogenesis through FA overactivation of the sympathetic nervous system and subsequent portal hypertension and signaling of HSC activation [6]. Additionally, research has shown that alcoholic fatty liver disease (AFLD) correlates with enhanced susceptibility of the liver to endotoxin-induced fibrogenic changes after chronic ethanol consumption due to disruption of intestinal permeability and increased pro-inflammatory cytokine production in macrophages and other infiltrating immune cells [4]. Tumor necrosis factor (TNF)-α, the major pro-inflammatory cytokine in ALD, increases the rate of FA synthesis and liver injury through activation of lipid-metabolism regulators such as sterol regulatory element-binding protein (SREBP)-1 and early growth response (Egr)-1 [4, 7]. In fact, Laura Nagy's group demonstrated that Egr-1 is required for the full activation of TNFα in response to LPS, and not only does Egr-1 contribute to increased LPS sensitivity, but it is also required for the development of chronic ethanol-induced liver injury [8].

Egr-1 is an immediate early response gene that encodes a zinc finger-containing transcription factor [9]. Induced by a variety of stimuli such as cytokines, growth factors, tissue damage and ROS, Egr-1 is a key mediator in multiple processes, including inflammation, angiogenesis, and extracellular matrix remodeling, which are involved in fibrosis [10, 11]. Regulation of genes such as vascular endothelial growth factor (VEGF) in angiogenesis and TNFα in inflammation support a positive role of Egr-1 in the regulation of the wound healing response. More importantly, control of the profibrotic cytokines transforming growth factor (TGF)-β, platelet-derived growth factor (PDGF), and fibroblast growth factor (FGF) suggest that Egr-1 is required for fibrosis in response to liver injury [12]. Indeed, Egr-1 has been shown to play a role in regulating fibrosis in various mouse models of human disease. For instance, Egr-1 was elevated in livers from mice after bile duct ligation, a model of cholestatic liver injury [13]. Consistently, Egr-1 deficiency protected against bleomycin-induced dermal and lung fibrosis as well as LPS/galactosamine-induced liver injury [14-16]. In contrast, Egr-1 deficiency worsened fibrosis in a model of xenobiotic-induced cholestasis in mice independent of changes in injury or inflammation [17]. Similarly, recent studies have shown that carbon tetrachloride (CCl_4)-induced hepatic fibrosis was enhanced, not attenuated, in mice lacking Egr-1 [18, 19]. In consequence, the function of Egr-1 in fibrosis remains poorly understood, and further investigation into the effects of Egr-1 deficiency on hepatic fibrosis could help to better understand how Egr-1 may be used as a potential target for the development of anti-fibrotic interventions.

In this study, we hypothesized that the loss of Egr-1 exacerbates CCl_4-induced liver injury, which subsequently contributes to the progression to fibrosis. Making use of

Egr-1 deficient mice, we investigated whether the loss of Egr-1 would contribute to injury, steatosis, and the appearance of early markers of fibrosis using a model of moderate ethanol feeding to accelerate CCl_4-induced fibrogenesis paralleling the acceleration of fibrosis by ethanol in wild-type mice shown previously by Roychowdhury *et. al* [20]. While Egr-1 deficiency had no effect on CCl_4-mediated hepatic injury, steatosis and expression of early fibrosis markers was increased in *Egr-1 -/-* mice and ethanol feeding worsened this effect demonstrating a protective role of Egr-1 in the development of liver fibrosis.

Our overall hypothesis was that Egr-1 contributes to the attenuation of hepatic fibrosis, and this was tested as defined briefly in the following specific aims.

Specific Aim 1: Determine the effects of Egr-1 on the induction of early markers of fibrosis. Based on previous work illustrating that Egr-1 is a negative regulator of chronic CCl_4-induced hepatic fibrosis and the oval cell response [18], we tested the hypothesis that Egr-1 attenuates, not exacerbates, hepatic fibrogenesis. We tested this hypothesis using a model of ethanol-accelerated, CCl_4-induced liver injury to stimulate fibrogenesis in wild-type and Egr-1 deficient mice. Consequently, we measured changes in liver injury by ALT and AST; changes in steatosis by hepatic triglyceride content, and fibrogenic changes as measured by transcript and protein levels of common markers of fibrogenesis.

Specific Aim 2: Identify gene targets of Egr-1 that may contribute to the Egr-1-mediated effects on fibrogenesis. Reactive oxygen species (ROS) are a product of both ethanol metabolism and CYP2E1-mediated bioactivation of CCl_4. Since Egr-1 is rapidly and transiently induced in the presence of ROS and oxidative damage, we tested the hypothesis that Egr-1 regulates antioxidant genes, which may play an essential role in the attenuation of hepatic fibrosis. To the test this hypothesis, we followed up on the results of an SA Biosciences Oxidant Stress, Antioxidant Defense Pathway array with real-time PCR and Western blot analysis. Chromatin immunoprecipitation was subsequently performed to investigate the relationship between Egr-1 and a suspected gene target, NAD(P)H dehydrogenase, quinone 1 (Nqo1).

Specific Aim 3: Define mechanisms by which Egr-1 exerts inhibitory effects on liver disease progression. To determine the mechanism by which Egr-1-mediated induction of Nqo1 protects against ethanol-fed, CCl_4-induced liver injury, we explored the different

functions of Nqo1. To investigate effects of Egr-1 deficiency on oxidative damage, we quantified oxidative stress by immunohistochemistry of 4-hydroxynonenal (4-HNE), glutathione depletion assay, and assay of cellular total antioxidant capacity in wild-type and *Egr-1* -/- mice after ethanol feeding and CCl_4 exposure. We also performed histological quantification of abnormal mitotic figures and measurement of cellular NAD+/NADH ratios.

Materials and Methods

Antibodies: 4-HNE (Alpha Diagnostic, San Antonio, TX), Nqo1 and α-smooth muscle actin (αSMA) (clone 1A4) (Sigma-Aldrich, St. Louis, MO), Egr-1 (clone 15F7) and GAPDH (clone 14C10) (Cell Signaling, Danvers, MA), and RNA polymerase II (Millipore, Darmstadt, Germany).

Animals and Experimental Design

All experiments were conducted with the approval of the Institutional Animal Care and Use Committee at the University of Kansas Medical Center. Mice deficient in *Egr-1* were bred from male and female heterozygotes (*Egr-1 +/-*) on a C57BL/6 Taconic background; wild-type control mice were littermates of *Egr-1 -/-* mice. Ten to 12-week-old female *Egr-1 +/+* and *Egr-1 -/-* mice were housed in ventilated cages on a 10/14h light and dark cycle in 50% humidity. Animals were grouped 2 per cage, and those on control diet were paired to ethanol-fed animals to equalize caloric intake between groups for the following experiment.

Model of Ethanol-accelerated, CCl_4-induced fibrogenesis: Using methods previously described [20], mice were acclimatized to a liquid diet for 2 days, and subsequently fed increasing concentrations of ethanol (1 to 2% v/v) for 2 days each. Lieber-DeCarli high fat ethanol and control diets were obtained from Dyets (Bethlehem, PA). After two days of 2% ethanol feeding, mice were injected with CCl_4 (0.4mg/g bw, diluted 1:3 in olive oil) or olive oil alone for control [21]. Mice continued on pair and ethanol-containing diets until euthanized 48 and 72hr after CCl_4 injection. Mice were euthanized 12hr post CCl_4 for 4-HNE immunohistochemistry.

β-Lapachone administration: β-Lapachone (β-L) purchased from Abcam (Cambridge, MA) was dissolved in DMSO (8mg/mL) and injected i.p. at 20mg/kg in 100mg/kg of hydroxypropyl-β-cyclodextrin (CTD Holdings, Inc., Alachua, FL) to increase bioavailability and solubility [22]. The first β-L injection occurred 12hr prior to CCl_4 administration, and was given once daily until mice were euthanized 72hr after CCl_4 exposure.

For euthanasia, mice were anesthetized with a cocktail of 107.2mg/kg ketamine, 4.29mg/kg xylazine, and 3.55mg/kg acepromazine; blood was taken from the vena cava and collected into EDTA-containing tubes supplemented with aprotinin to obtain plasma. The liver was excised, sectioned, snap frozen in liquid nitrogen, and stored at -80°C. Separate liver pieces were formalin-fixed and paraffin-embedded for further histological analysis, or saved in RNAlater® solution (Life Technologies, Grand Island, NY) for RNA isolation and cDNA synthesis.

Hepatic stellate cell (HSC) isolation: Here, animals were euthanized by cervical dislocation. Livers were harvested and placed into 25mL of Hanks balanced salt solution (HBBS) deficient in Ca^+ and Mg^+ (Gibco®, Life Technologies). In a culture hood, livers were washed 2-3 times in HBBS deficient in Ca^+ and Mg^+ to remove blood. After the final wash, livers were minced and transferred to individual 250mL Nalgene flasks with 10mL of enzyme solution (3.75mg/mL pronase, 0.5mg/mL collagenase, and 0.1mg/mL Dnase I in HBBS deficient in Ca^+ and Mg^+). Flasks were then incubated in a water bath at 37°C, shaken at 100rpm. Digests were poured through a Cellector (#30 metal mesh insert, Bellco Glass, Vineland, NJ) into 50mL centrifuge tubes. Final volumes were brought to 50mL with HBBS deficient in Ca^+ and Mg^+ and tubes were centrifuged at 50 x

g for 5min at 4°C to pellet hepatocytes and red blood cells. Supernatants containing non-parenchymal cells (NPC) were transferred to new 50mL centrifuge tubes and final volumes were brought to 50mL with HBBS deficient in Ca^+ and Mg^+. Tubes were then centrifuged at 1,000 x g for 6min at 4°C to pellet remaining NPC. All but 5mL of supernatant was removed, and NPC pellets were resuspended in the remaining supernatant. To each tube, 30mL of HBBS deficient in Ca^+ and Mg^+ was added with 400µL of Dnase I and centrifugation at 1,000 x g for 6min at 4°C was performed. After removal of supernatants, pellets were resuspended in 2.5mL of HBBS deficient in Ca^+ and Mg^+ and 2mL of 3g/L Ultra Fatty Acid Free BSA (Roche) was added. Samples were transferred to 15mL centrifuge tubes, and 4mL of 28.7% Histodenz (Sigma-Aldrich) in HBBS deficient in NaCl was added. Subsequently, 3mL of HBBS with 3g/L BSA was added slowly to maintain a sharp interface between the sample and the HBBS. Following centrifugation at 2,500 x g for 17min at 4°C, the opaque interface containing HSC was transferred to pre-chilled 15mL centrifuge tubes containing 5mL of Dulbeco's Modified Eagle's medium (DMEM) with 20% fetal bovine serum (FBS). Additional centrifugation was performed at 1,000 x g for 5min at 4°C, and supernatants were discarded. Pellets were resuspended in 1mL DMEM and 20% FBS, and 10µL of resultant cells were mixed with 40µL of trypan blue for cell counting. Cells were diluted for plating at 250,000cells/cm^2, and 24 hours later, medium was changed to eliminate non-adherent cells. Cells were harvested 5, 7, and 10 days after plating for subsequent RNA and protein analysis.

RNA Isolation and PCR

RNA was isolated from liver using the Qiagen RNeasy Mini Kit or from HSC with the Qiagen RNeasy Micro Kit (Valencia, CA). Reverse transcription and cDNA synthesis was performed with the use of the RETROscript® kit from Ambion, Inc (Grand Island, NY). Real-time polymerase chain reaction (real-time PCR) was performed using a Real-time PCR CFX384 plate reader (BioRad, Hercules, CA) with primers specific to genes of interest; 18S was used for normalization. All primers were obtained from Integrated DNA Technologies (IDT) (Table 1). Data collected was analyzed using the Livak method where the resultant Ct value represented the cycle at which a threshold was reached per gene of interest. Calculation of ΔCt was performed by subtracting the Ct for 18S from the Ct for the gene of interest, and ΔΔCt was calculated by subtracting the ΔCt of each treatment group from the ΔCt of the control group. Fold changes were calculated as $2^{-\Delta\Delta Ct}$.

Table 1. List of primer sequences used for real-time PCR analysis.

Gene Name	Forward Primer	Reverse Primer
18S	ACGGAAGGGCACCACCAGGA	CACCACCACCCACGGAATCG
Egr-1	GCCTCGTGAGCATGACCAAT	GCAGAGGAAGACGATGAAGCA
Col1a1	ATGTTCAGCTTTGTGGACCTC	CAGAAAGCACAGCACTCGC
Acta2	GTCCCAGACATCAGGGAGTAA	TCGGATACTTCAGCGTCAGGA
Nqo1	AGGATGGGAGGTACTCGAATC	TGCTAGAGAGATGACTCGCTATTT
Ces1 d	GAGACCCAAGGCAGTAATAGGA	GAGTGGAGGCACCAATCTTCA
Pnpla3	ATGGACCTCGTGCGGAAAG	CCTGGAGCCCGTCTCTGAT
Nqo1 (ChIP)	TGCCTACATAATCAGCCTGTG	AATTTGAGCCCATCCGTTTTG

Western Blotting

Protein lysates were made from liver pieces between 50-100mg. Liver pieces were homogenized in 1X RIPA buffer with added proteinase inhibitors in pre-filled bead homogenization tubes (Wisbiomed, San Mateo, CA) at 4m/s for 45sec in a bead homogenizer (Fast Prep 24, MP Biomedicals, Solon, OH). After centrifugation at 21,000 x g for 15min at 4°C, supernatants were diluted 1:30 in water and the Pierce® BCA assay (Thermo Scientific, Waltham, MA) was used to determine protein concentrations. Forty micrograms of protein was loaded onto a 10% polyacrylamide gel and electrophoresed at 125V for 85 minutes. Protein was transferred to a PVDF membrane at 0.04A for 75 minutes. Membranes were blocked in 5% BSA in Tris-buffered saline with 0.1% Tween 20 (TBST) for an hour at room temperature, then incubated with primary antibody overnight at 4°C on an orbital shaker. Primary antibodies were diluted in 1% BSA in TBST and 0.02% sodium azide at 1:5,000 for anti-Nqo1, 1:2,000 for anti-Hsp47, and 1:1,000 for anti-αSMA. Secondary antibody incubation was done at 1: 20,000 in 3% BSA in TBST for an hour at room temperature. GAPDH was used as the loading control for all proteins of interest. Immunodetection was done by chemiluminescence using Amersham ECL™ Western blotting kit (GE Healthcare).

HNE Immunohistochemistry

Formalin-fixed, paraffin-embedded tissue was deparaffinized and stained for 4-HNE using a protocol outlined by Gavin Arteel [23]. The primary antibody was diluted 1:250 in 1% BSA in phosphate-buffered saline with 5% Tween 20 (PBST), and immunohistochemical detection was done using the Dako EnVision Kit (Carpinteria, CA).

Plasma ALT/AST Activity Assay

ALT and AST assays were performed on isolated plasma samples with kits from Sekisui Diagnostics (Lexington, MA). Plasma samples were diluted in saline based on previous data collected in the lab. In a UV-invisible 96-well plate, 10μL of each diluted sample was added in duplicate (5μL for AST activity assay). Subsequently, 90μL of ALT reagent (1 part reagent 1 to 4 parts reagent 2) was added to each well (100μL of AST reagent), and absorbance readings were taken every 30sec over 5min at 340nm.

Hepatic Triglyceride Measurement

Total hepatic triglyceride levels were measured using reagents purchased from Pointe Scientific, Inc (Canton, MI). Liver pieces between 75-95mg were digested in 3M KOH in 65% ethanol at 70°C for an hour. Following 24hr incubation at room temperature, sample volumes were brought to 500μL with 2M Tris-HCl, pH 7.5. Samples were then diluted 1:5 in separate tubes containing 400μL of 2M Tris-HCl, pH 7.5, and 10μL of diluted sample was added to 1mL of prewarmed (37°C for 5min) GPO liquid reagent. Different volumes (0, 0.63, 1.25, 2.5, 3.75, 5, 7.5, 10, 20, and 40μL) of GPO standard reagent were added to prewarmed 1mL tubes of GPO liquid reagent to create a standard curve. After a second incubation at 37°C for 5min, 200μL of each standard and sample was added to a 96-well plate in duplicate. Absorbances were read at a wavelength of 500nm and adjusted for the absorbance of water, which was used as a blank. Total hepatic triglyceride content was calculated using the linear equation generated by the standard curve.

CYP2E1 Activity Assay

Using methods modified from those described previsouly [24], samples were homogenized in ice-cold PBS and centrifuged for 15min at 9,000 x g at 4°C.

Supernatants were ultracentrifuged at 105,000 x g for an hour at 4°C to isolate microsomal fractions. Microsomes were diluted in 0.15M KCl and assayed in a 100μL reaction mixture of 10mM p-nitrophenol, phosphate buffer, NADPH, and 100μg of protein. Protein normalization was determined by BCA assay. After an hour, the reaction was stopped with 20% TCA, and CYP2E1 activity, measured in 10N NaOH, was read at a wavelength of 510nm.

Nqo1 Activity Assay

Nqo1 activity was determined using a previously described protocol [25]. Briefly, liver samples were homogenized in a sample buffer of 25mM Tris-HCl, 250mM sucrose, and 1μM FAD, pH 7.4. Following centrifugation at 10,000 x g for 5min at 4°C, supernatants were ultracentrifuged at 120,000 x g for an hour at 4°C to collect cytosolic fractions. In a reaction mixture of 500μM NADPH, 40μM DCPIP, 50mM Tris-HCl, and 20μg of protein Nqo1 activity was assayed over 5 minutes at 27°C at a wavelength of 600nm.

Chromatin Immunoprecipitation

To investigate the interaction between Egr-1 and the *Nqo1* promoter, around 200mg of mouse liver was homogenized in 1mL of cell lysis buffer (10mM Tris-HCl, 10mM NaCl, 3mM $MgCl_2$, 0.5% NP-40) containing protease inhibitors (10μL/mL). Crosslinks were formed between protein and DNA using 25μL of 10% buffered formalin phosphate with rotation at room temperature for 30 minutes. Glycine (100μL), with an additional 5 minutes of rotation, was used to stop crosslinking. After centrifugation at 2,000 x g for 2 minutes at 4°C, nuclei were lysed with resuspension of resultant pellet in 1mL of nuclear lysis buffer (0.2% SDS, 5mM EDTA, 50mM Tris-HCl) containing protease inhibitors. Chromatin was then sheared to 200-1000bp by sonication, and sonication efficiency was

determined by gel electrophoresis. Subsequently, 50μg of chromatin was pre-cleared for an hour with rotation at 4°C in Invitrogen Dynabeads, then immunoprecipitated overnight with Egr-1 antibody, RNA Polymerase II antibody as a positive control, or no antibody as a negative control. Following overnight incubation, washed Dynabeads were added to each sample to isolate antibody-bound chromatin, and beads were subsequently washed in a ChIP low-salt buffer (0.1% SDS, 1% Triton X-100, 2mM EDTA, 50mM Hepes, 150mM NaCl), ChIP high-salt buffer (same as low-salt buffer, but with 500mM NaCl), ChIP LiCl buffer (0.25mM LiCl, 0.5% NP-40, 0.5% Na-deoxycholate, 1mM EDTA, 10mM Tris-HCl), and TE buffer (10mM Tris-HCl, 1mM EDTA), consecutively. Chromatin was then eluted and crosslinks reversed by incubation overnight at 65°C. DNA was then purified via phenol:chloroform extraction and analyzed by real-time PCR using primers specific to the *Nqo1* promoter.

Glutathione (GSH) Measurement

GSH levels were measured using a previously described protocol [26], in which frozen liver sections were homogenized in 3% sulfosalicylic acid with 0.1mM EDTA. To determine total glutathione, homogenates were diluted in 0.01N HCl, centrifuged at 18,000 x g for 4min at 4°C, and further diluted in potassium phosphate buffer (KPP). To determine glutathione disulfide (GSSG), homogenates were diluted in N-ethylmaleimide (NEM) and KPP. NEM served to trap GSH to isolate GSSG in solution. Absorbances were measured in a test solution of 5,5'-Dithio-bis(2-nitrobenzoic acid) (DTNB) at a wavelength of 412nm.

Total Antioxidant Capacity Assay

Total antioxidant capacity was quantified with the use of Cell BioLab's Oxiselect™ TAC assay kit per manufacturer-provided protocol. Liver samples were homogenized in cold PBS with the use of an automated bead homgenizer (Fast Prep 24) and centrifuged at 10,000 x g for 10min at 4°C. In a 96-well microtiter plate, 20μL of freshly made diluted uric acid standard and supernatant from each sample was added in duplicate. To each well, 180μL of 1X Reaction Buffer was added using a multichannel pipette and mixed thoroughly. Following an initial absorbance read at 490nm, the reaction was initiated with the addition of 50μL of 1X Copper Ion Reagent and incubated for 5min on an orbital shaker. The reaction was terminated upon addition of 50μL of 1X Stop Solution and a final absorbance read was again measured at 490nm.

NAD+/NADH Quantification

With the use of an NAD+/NADH quantification colorimetric kit obtained from BioVision (Milpitas, CA), samples were assayed per manufacturers instructions. Liver was homogenized in 400μL of NADH/NAD extraction buffer. Following centrifugation at 18,400 x g for 5min, half the supernatant was transferred to a new tube and incubated at 60°C for 30min to decompose NAD. Samples containing total NAD and NADH alone were diluted in NADH/NAD extraction buffer and assayed in a mixture of NADH cycling buffer, NADH cycling enzyme mix, and NADH developer. Absorbances were read at a wavelength of 450nm and compared to a standard curve provided by the manufacturer.

Statistical Analysis

Densitometry of immunoblots and quantification of immunohistochemistry was done with the use of ImageJ [27]. Statistical analysis was performed by ANOVA post hoc analysis using Tukey's adjustment for multiple measures on SAS. For CYP2E1 activity and β-Lapachone experiments, the student's t-test was used for analysis. All data are represented as the mean ± the standard error of the mean (SEM). For all instances, $N \geq 4$ mice per experimental group where * denotes different than wild-type and ** denotes different in *Egr-1 -/-* between pair and ethanol-fed knockouts and ethanol-fed wild-type at the same time point. Significance was taken to be $p<0.05$.

Results

Ethanol feeding reduces Egr-1 and exacerbates the appearance of early markers of fibrosis. Egr-1 is implicated in the pathogenesis of fibrosis in models of lung fibrosis and scleroderma [15]; however, it remains unclear what happens to Egr-1 after moderate ethanol feeding and CCl_4 exposure and how its expression affects the progression of hepatic fibrosis. We found that 48h after a single CCl_4 injection, which initiates the appearance of hepatic fibrosis, there was a 50% reduction in the transcript levels of *Egr-1* with ethanol feeding (Fig. 1A). By 72h, *Egr-1* mRNA levels in both pair and ethanol-fed mice returned nearly to baseline. Interestingly, Egr-1 protein was stabilized up to 72h after CCl_4 injection, but ethanol feeding inhibited this effect.

To investigate the effects of *Egr-1* deficiency on hepatic fibrosis, we examined the expression of Col1a1 and αSMA in whole liver from *Egr-1* +/+ and *Egr-1* -/- mice 72h after CCl_4 exposure (Fig. 2). Hepatic stellate cells (HSC), the main cell type responsible for hepatic fibrosis, excessively deposit type I collagen and express αSMA during progression of the disease. To date, these genes are commonly used as markers of HSC activation. In our studies, we found that not only was Col1a1 and αSMA mRNA increased 72h after CCl_4, but we also found that the loss of *Egr-1* exacerbated this induction (Fig. 2A). Although the data are not significant for Col1a1, ethanol feeding further heightened the induction of αSMA mRNA after CCl_4 (Fig. 2A). Similarly, immunoblotting for αSMA demonstrated the same pattern of expression (Fig. 2B). We also examined transcript levels of these genes within HSC isolated from wild-type and *Egr-1* -/- mice, and consistently discovered that as these cells spontaneously activate in culture over time there was an induction of Col1a1 and αSMA in wild-type HSC that was

enhanced in *Egr-1 -/-* HSC. Together, these data demonstrate an accelerated profibrotic phenotype in CCl_4 exposed, *Egr-1 -/-* mice that is worsened with ethanol feeding, and this suggests that Egr-1 attenuates, not exacerbates, fibrogenic changes in the liver after ethanol feeding and CCl_4 exposure.

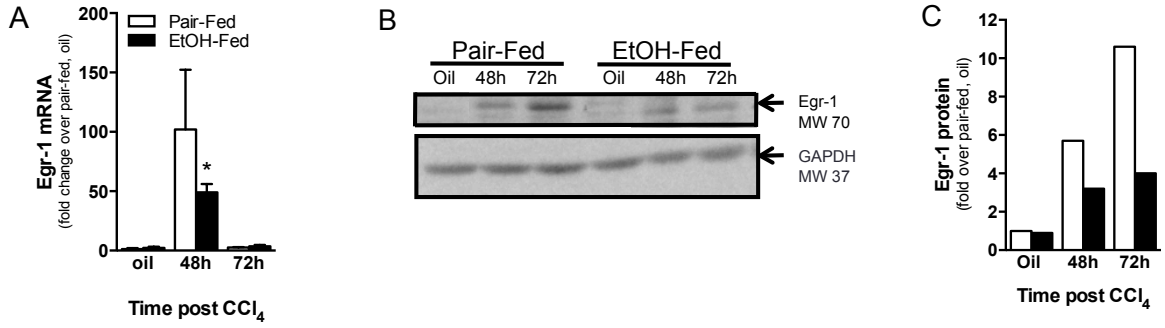

Figure 1. Ethanol feeding reduces Egr-1 mRNA and protein levels. (A) Real-time PCR was performed on livers from pair and ethanol-fed mice 48 and 72h after CCl_4 to measure transcript levels of Egr-1. (B) Egr-1 protein content was determined by Western blot from pooled mouse liver samples. Densitometric analysis of Western blot data was performed using ImageJ; GAPDH was used as a loading control.

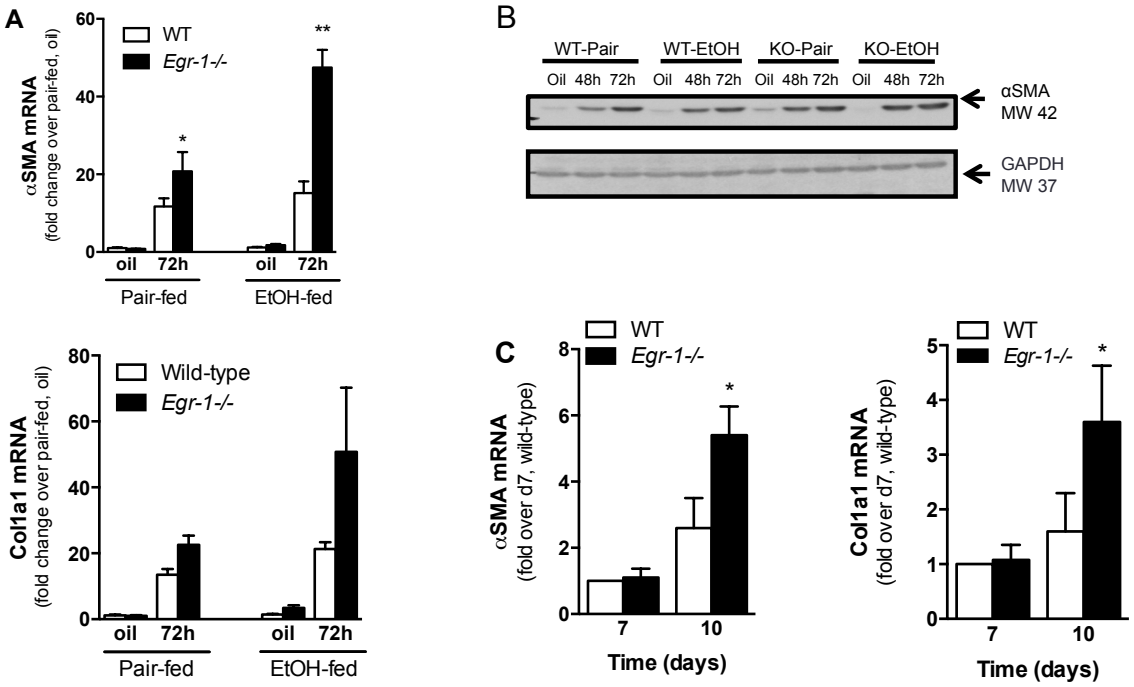

Figure 2. Ethanol feeding increases hepatic accumulation of fibrotic markers from CCl_4-treated, Egr-1-deficient mice. Real-time PCR was used to determine hepatic (A) αSMA and Col1a1 transcript level. (B) Western blotting on pooled liver homogenates was used to determine αSMA protein quantity; GAPDH was used as a loading control. Consistently, real-Time PCR shows enhanced expression of fibrosis markers in hepatic stellate cells (C).

Egr-1 deficiency and ethanol feeding delay recovery from CCl_4-induced steatosis, independent of liver injury. As the first in a spectrum of liver pathologies that arise from chronic alcohol consumption, steatosis can predispose patients to liver disease progression. Since our data suggest that the loss of *Egr-1* increases fibrogenesis in the liver after CCl_4 and ethanol feeding, we hypothesized that Egr-1 deficiency would also lead to an increase in steatosis. First, in an effort to rule out the possibility that the accelerated profibrotic phenotype seen in *Egr-1 -/-* mice was due to enhanced liver injury, we measured the severity of liver injury after CCl_4 exposure by plasma alanine aminotransferase (ALT) and aspartate aminotransferase (AST) activities (Fig. 3A). At the

time of peak injury following CCl_4 (48h), markers of liver injury showed no difference between genotypes or diets (Fig. 3A).

Second, we examined steatosis by measuring hepatic triglyceride levels and found that steatosis was increased in both genotypes after CCl_4 (Fig. 3B); however, triglycerides remained elevated in *Egr-1 -/-* mice while this level was reduced to baseline in wild-type mice at 72h. Ethanol feeding further increased hepatic triglyceride accumulation.

Lastly, similar to Roychowdhury *et. al* [20], we sought to confirm that moderate ethanol used in this model did not increase the bioactivation of CCl_4. Chronic ethanol consumption induces the cytochrome P450 enzyme CYP2E1. CYP2E1 contributes to the metabolism of ethanol, and is the same enzyme that metabolizes the bioactivation of CCl_4. Therefore, high concentrations of ethanol can induce *CYP2E1*, and thus increase the bioactivation of CCl_4 into its reactive metabolites, accelerating fibrogenesis. However, the use of 2% ethanol in this animal model showed no differences in CYP2E1 activity between wild-type and *Egr-1 -/-* and pair and ethanol-fed mice (Fig. 3C). This suggests that the enhanced fibrogenic changes seen in the *Egr-1 -/-* mice are independent of differences in liver injury and CYP2E1-mediated bioactivation of CCl_4. Collectively, these data support the hypothesis that in addition to attenuating fibrogenic changes in the liver after CCl_4, Egr-1 also contributes to resolution from CCl_4-induced hepatic steatosis.

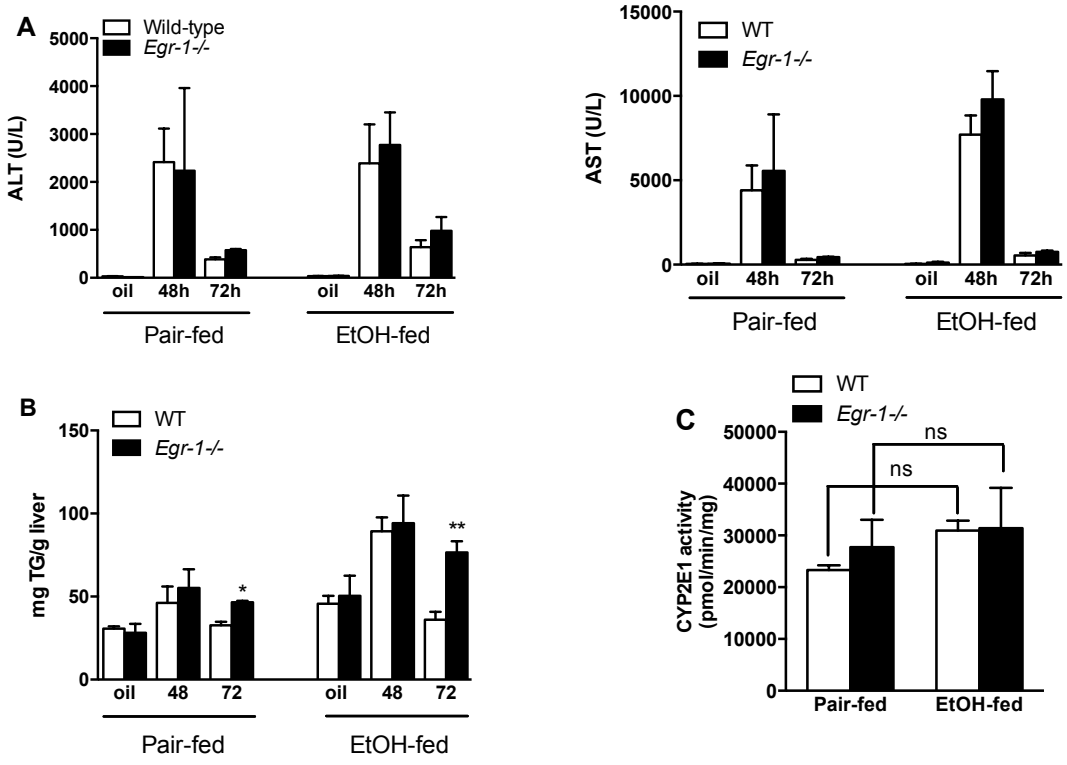

Figure 3. Enhanced fibrogenic changes in *Egr-1 -/-* mice are independent of increased liver injury and CCl_4 bioactivation. Plasma ALT and AST activities (A) and hepatic triglyceride (B) were determined 48 and 72h after CCl_4. These data are independent of differences in CYP2E1-mediated bioactivation of CCl_4 (C); ns denotes no significance.

Loss of Egr-1 inhibits the induction of *Nqo1* after ethanol feeding and CCl_4 exposure. Egr-1 is a redox-sensitive transcription factor that is highly inducible by a variety of stimuli including cellular oxidative stress [28]. In CYP2E1-mediated metabolism of ethanol, the use of oxygen to metabolize alcohol can lead to the generation of reactive oxygen species (ROS). CYP2E1 can also catalyze the formation of an ethanol-derived free radical, which also contributes to oxidative damage [29]. Similarly, metabolism of CCl_4 by CYP2E1 leads to the formation of reactive metabolites, such as CCl_3• and CCl_3OO•, which can bind to cellular macromolecules, including lipids, leading to lipid peroxidation and the formation of ROS. Therefore, we sought to test the

hypothesis that Egr-1 attenuates hepatic fibrosis through augmentation of antioxidants, such that the loss of Egr-1 leads to a loss in antioxidant expression and increased fibrogenesis. An SA Biosciences Oxidant Stress, Antioxidant Defense Pathway array was performed on liver from ethanol-fed, wild-type and *Egr-1 -/-* mice 72h after CCl_4 to elucidate previously unrecognized antioxidant gene targets of Egr-1 (Table 2). Surprisingly, the expression of superoxide dismutase (SOD) 1 and 2, known gene targets of Egr-1, remained unchanged. However, there was significant reduction in the expression of other antioxidants such as glutathione peroxidase (Gpx) 2, thioredoxin (Txnip), sulfiredoxin (Srxn) 1, and NAD(P)H dehydrogenase, quinone 1 (Nqo1). Subsequent validation by real-time PCR confirmed the loss of Nqo1 mRNA and protein in ethanol-fed, *Egr-1 -/-* mice after CCl_4 (Fig. 4A-B). Interestingly, examination of *Nqo1* transcript levels in isolated HSC found that wild-type mice showed a decrease in *Nqo1* mRNA over the course of plate-induced activation while *Egr-1 -/-* mice had significantly less *Nqo1* that did not change over time in culture (Fig. 4C). Together, these data indicate that Egr-1 regulates *Nqo1,* whether through a direct or indirect relationship, however, remains unclear.

Egr-1 recognizes and binds DNA at a GC-rich consensus sequence identified as 5'-GCGTGGGCG-3' [30]. *In silico* analysis revealed a potential Egr-1 DNA binding site in the *Nqo1* promoter, less than 1Kb upstream of the transcriptional start site (TSS) (Fig. 5A). To more closely explore the relationship between Egr-1 and the *Nqo1* promoter, chromatin immunoprecipitation (ChIP) was performed in liver samples at baseline and 2h following CCl_4 administration—when Egr-1 induction is the highest (Fig. 5B). Analysis by real-time PCR confirmed that Egr-1 was absent from the *Nqo1* promoter at baseline

when Egr-1 was not expressed, and at peak Egr-1 induction there was indeed an association of Egr-1 to the promoter region. These data demonstrate direct DNA binding of Egr-1 to the *Nqo1* promoter, where the loss of Egr-1 results in reduced expression of Nqo1, and introduce *Nqo1* as a novel antioxidant gene target of Egr-1.

Table 2: Oxidant Stress and Anti-Oxidant Pathway Array (wt vs *Egr-1-/-* after EtOH & CCl_4 exposure)

Layout	1	2	3	4	5	6	7	8	9	10	11	12
A	Gpx8 **2.06**	Aass **2**	Als2 **-2**	Apc **2**	Apoe **1.01**	Aqr **2.05**	Atr **-1.98**	Cat **-1.99**	Ccs **1**	Xirp1 **1.01**	Ctsb **1.01**	Cyba **1**
B	Cygb **2**	Dnm2 **2.01**	Duox1 **1.01**	Ehd2 **-1.01**	Epx **1.01**	Ercc2 **1.01**	Ercc6 **2.01**	Fancc **1.01**	Fmo2 **2.03**	Gab1 **-1**	Gpx1 **1.02**	Gpx2 **-7.98**
C	Gpx3 **2.02**	Gpx4 **-1**	Gpx5 **1.01**	Gpx6 **2.04**	Gpx7 **1.01**	Gsr **-1.98**	Gstk1 **1**	Hbq1a **1.01**	Idh1 **-1.98**	Ift172 **1.01**	Il19 **1.01**	Il22 **1.01**
D	Kif9 **1.01**	Lpo **1.01**	Mb **1.01**	Mpo **-1.06**	Mpp4 **1.01**	Ncf2 **2.05**	Ngb **1.01**	Nos2 **1.03**	Nox1 **1.01**	Nox4 **2.01**	Noxa1 **2.05**	Noxo1 **2.03**
E	Nqo1 **-3.97**	Nudt15 **1**	Nxn **4.14**	Park7 **2.02**	Ppp1r15b **1.01**	Prdx1 **1.01**	Prdx2 **2.04**	Prdx3 **-1**	Prdx4 **1.01**	Prdx5 **2.02**	Prdx6 **2.03**	Prdx6-ps1 **1.01**
F	Prnp **2.01**	Psmb5 **1.01**	Ptgs1 **1**	Ptgs2 **1.01**	Rag2 **1.01**	Recql4 **1**	Scd1 **-3.96**	Serpinb1b **-1.98**	Slc38a1 **-2.01**	Slc41a3 **2.02**	Sod1 **1.01**	Sod2 **-1**
G	Sod3 **1.02**	Srxn1 **-3.96**	Tmod1 **1.01**	Tpo **1.01**	Txnip **-32.84**	Txnrd1 **-1.97**	Txnrd2 **1.02**	Txnrd3 **2.02**	Ucp3 **1.01**	Vim **2.03**	Xpa **1.01**	Zmynd17 **1**

Table 2. An SA Biosciences Oxidant Stress, Antioxidant Defense Pathway array elucidated reduced antioxidants in ethanol-fed, CCl_4-exposed *Egr-1 -/-* mice. Boxes in yellow indicate known antioxidant gene targets of Egr-1; fold changes show no change in expression. Boxes in red indicate previously unidentified gene targets of Egr-1 that are significantly reduced 72h after CCl_4.

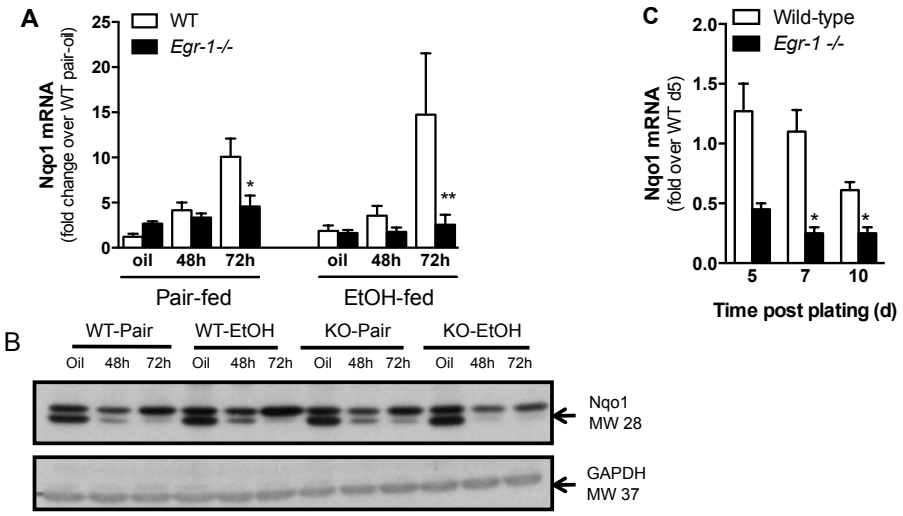

Figure 4. Egr-1 deficiency results in loss of *Nqo1* mRNA and protein in whole liver and HSC. (A) Real-time PCR analysis on whole liver 48 and 72h after CCl_4 shows there is a loss of Nqo1 induction, which is worsened with ethanol feeding. (B) Western blot analysis of Nqo1 protein levels. (C) HSC isolated from wild-type mice show a slight decrease in Nqo1 mRNA over the course of plate-induced activation ($p = 0.06$ at 72h). *Egr-1-/-* mice always have less Nqo1, but this does not change over time in culture.

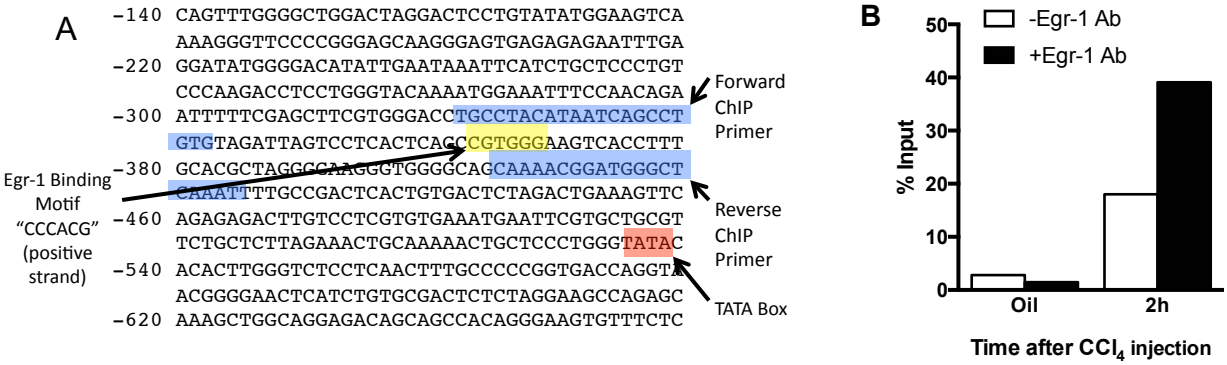

Figure 5. Chromatin immunoprecipitation confirms association between Egr-1 and the *Nqo1* promoter. (A) *In silico* analysis of the *Nqo1* promoter identified a putative Egr-1 binding site (in yellow) less than 1Kb upstream of the transcription start site. Forward and reverse ChIP primers are highlighted in blue and the TATA box is highlighted red. (B) Preliminary work in CCl_4-exposed, chow-fed mice showed an association between Egr-1 and the *Nqo1* promoter 2h after CCl_4.

Oxidative damage after ethanol feeding and CCl_4 is independent of Egr-1-mediated reduction in Nqo1. Reactive oxygen species formed from CYP2E1-mediated byproducts of CCl_4 metabolism damage hepatocytes and are eventually released into the extracellular matrix where they can injure surrounding hepatocytes and stimulate the activation of HSC [31]. We hypothesized that Egr-1 deficiency would reduce antioxidant defense necessary to attenuate oxidative damage in parenchymal cells, and accelerate the appearance of fibrosis markers. Nqo1 is commonly recognized for its antioxidant capabilities. Known to reduce quinones to hydroquinones, Nqo1 bypasses the production of free radicals that result from one-electron reduction processes by utilizing a two-electron reduction pathway. Reportedly, this flavoprotein is also involved in scavenging and reducing superoxide [32]. Since there is no quinone generation during the metabolism of CCl_4, we took multiple approaches to measure the severity of oxidative stress in *Egr-1 -/-* mice compared to wild-type (Fig. 6).

First, immunohistochemistry of 4-hydroxynonenal (4-HNE) was performed to measure levels of lipid peroxidation after CCl_4 exposure. Lipid peroxidation, or the oxidative degradation of lipids, is a crucial step in the pathogensis of many diseases and it is commonly quantified by the presence of peroxidation byproducts—reactive aldehydes such as 4-HNE and malondialdehyde (MDA) [33]. Contrary to our hypothesis, Figures 6A and B show no difference in histological representation or quantification of 4-HNE immunological staining 12h after CCl_4, a time point when 4-HNE adducts remain detectable.

Second, we measured glutathione (GSH) levels in a glutathione depletion assay (Fig. 6C). Redox reactions that convert GSH to its oxidized state, glutathione disulphide

(GSSG), reduce organic peroxides formed by oxidative stress and play an important role in cellular detoxification [34]. During this process in which GSH is depleted from the cell, the ratio of GSSG/GSH can be used as an indicator of oxidative damage and recovery. Therefore, an increased GSSG/GSH ratio is considered indicative of increased oxidative stress. However, over time GSSG is converted back to GSH by glutathione reductase, which is constitutively active and inducible by oxidative stress. Unexpectedly, pair-fed, *Egr-1 -/-* mice showed an increased GSSG/GSH ratio, and thus lower levels of GSH at baseline. Moreover, ethanol appeared to decrease GSH at baseline in wild-type animals alone. Even so, GSSG/GSH ratios decreased and GSH levels recovered similarly in all groups 12h following CCl_4, negating the idea that the glutathione system is more overwhelmed in *Egr-1 -/-* mice.

Third, we used a Total Antioxidant Capacity assay kit to directly measure the antioxidant capacity of wild-type and *Egr-1 -/-* mouse livers 12h after CCl_4 (Fig. 6D). Typically, antioxidants eliminate free radicals through hydrogen atom transfer or single electron transfer mechanisms. This assay quantified the ability of cellular antioxidant enzymes to transfer one electron to reduce copper (II) to copper (I). Earlier time points (1, 2, and 6h) in wild-type mice showed a slight reduction in total antioxidant capacity up to 6h following CCl_4 that recovered to baseline levels by 12h (data not shown), consistent with patterns of lipid peroxidation. Comparatively, by 12h post CCl_4, not only were copper-reducing equivalents recovered to baseline in *Egr-1 -/-* mice, but also there was no difference between diets or genotypes. Collectively, these data imply that the loss of Nqo1 via Egr-1 deficiency neither increases oxidative stress nor reduces cellular antioxidant defense in *Egr-1 -/-* mice ensuing CCl_4 administration.

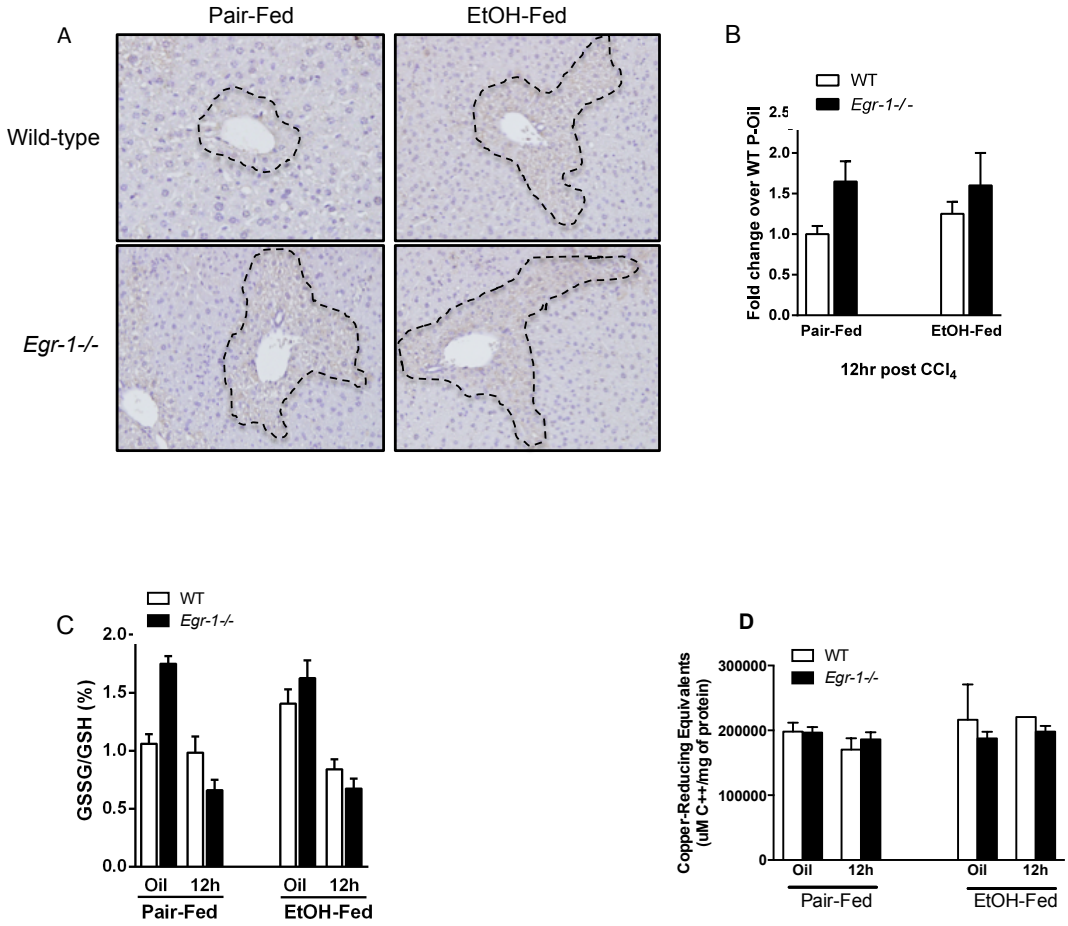

Figure 6. Reduced Nqo1 does not affect oxidative stress, cellular glutathione or total antioxidant capacity after CCl_4. Twelve hours post CCl_4, lipid peroxidation and glutathione levels were measured by immunohistochemistry of 4-HNE and a glutathione depletion assay, respectively (A-C). Total antioxidant capacity was assayed with the use of a kit that quantifies the capacity of antioxidant enzymes to reduce copper (II) to copper (I) (D).

Loss of Nqo1 does not affect mitotic spindle assembly. In addition to the role Nqo1 plays in attenuating oxidative damage, it is also associated with stabilizing microtubules of the mitotic spindle during mitosis [35, 36]. In particular, a role for Nqo1 in influencing microtubule polymerization was confirmed using inhibition studies in xenopus egg extracts [35], while confocal analysis demonstrated colocalization of Nqo1 with α-tubulin

in mitotic spindles of different human cell lines [36]. Consequently, since the above data demonstrated no change in oxidative stress with the loss of Nqo1, we ruled out Nqo1's antioxidant capacity as contributing to the reduced fibrogensis seen in wild-type mice compared to *Egr-1 -/-* mice. We subsequently explored the hypothesis that reduced Nqo1 leads to microtubule instability and abnormal mitotic spindle formation (e.g. tripolar spindles) resulting in apoptotic hepatocytes—stimuli for HSC activation. Quantification of mitotic figures was performed on hematoxylin and eosin stained histology sections from livers at baseline, 48 and 72h post CCl_4 (Fig. 7). Liver regeneration and entrance into the cell cycle did not begin until 48h after CCl_4 in wild-type mice, whereas *Egr-1 -/-* mice appeared to experience delayed mitosis, which was further inhibited by ethanol feeding (Fig. 7B). While *Egr-1 -/-* mice entered mitosis by 72h following CCl_4, they showed a lower number of cells in the mitotic phase of the cell cycle compared to wild-type, and the number of abnormal mitotic figures did not differ between genotypes (Fig. 7B-C).

The importance of Egr-1 in the regulation of entry into the cell cycle and mitotic progression has previously been reported in studies where Egr-1 null mice exhibited impaired liver regeneration after partial hepatectomy and acute CCl_4 exposure [21, 37]. Therefore, the reduced presence of mitotic figures in *Egr-1 -/-* mice seen here is not unexpected. However, these data suggest that loss of Nqo1 at the mitotic spindle in *Egr-1 -/-* mice does not affect the stability of the mitotic spindle nor the cell's ability to divide.

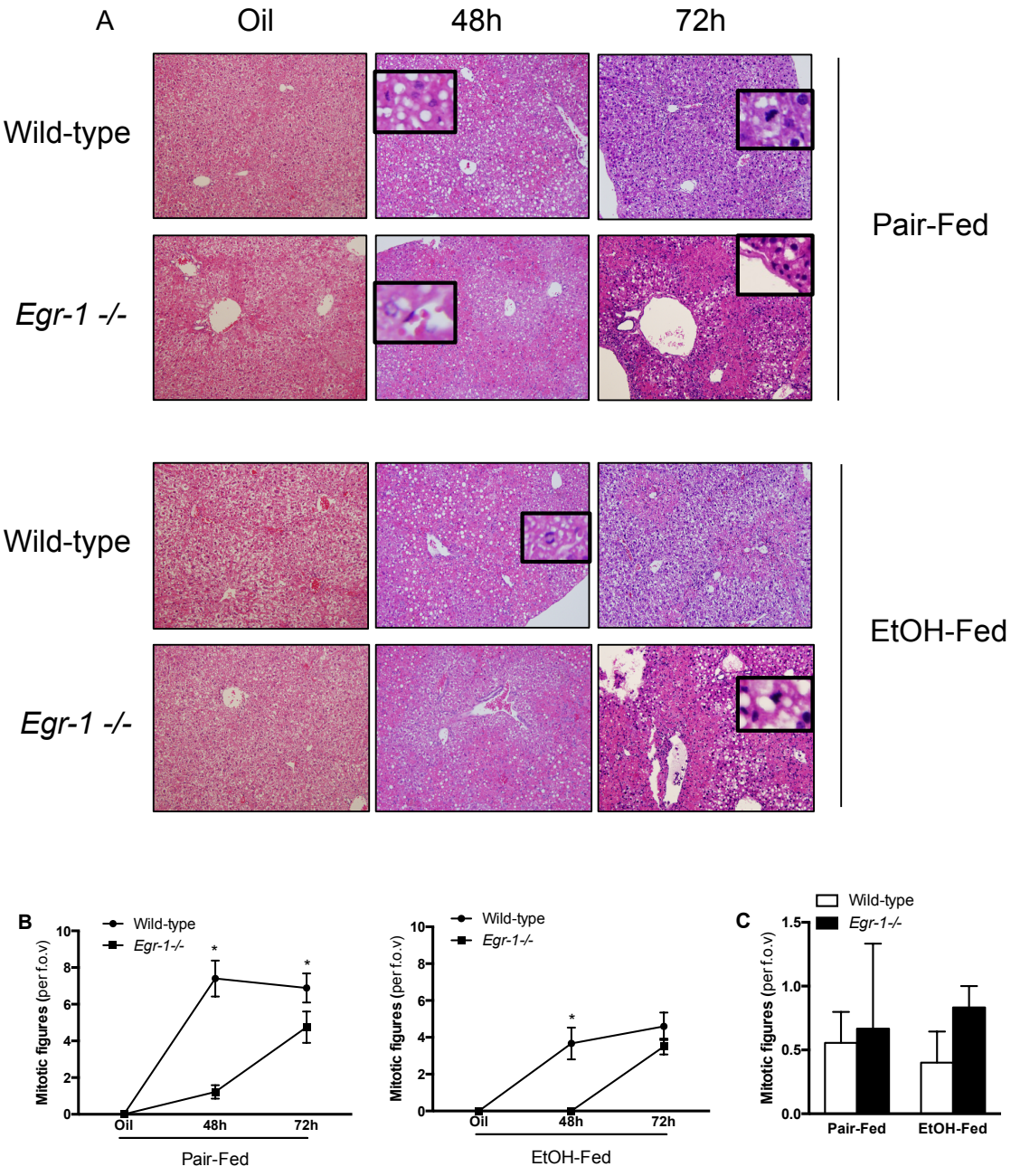

Figure 7. Loss of Nqo1 does not affect mitotic spindle assembly. (A) Hematoxylin and eosin-stained sections of wild-type and *Egr-1 -/-* liver at baseline, 48 and 72h post CCl_4. At 48h, examples of mitotic figures during metaphase and anaphase are designated in insets. At 72h, examples of abnormal mitotic spindles (e.g. tripolar spindles) are pictured in insets. (B) Quantification of mitotic figures averaged per field of view (f.o.v). (C) Graphical representation of abnormal or tripolar spindles per f.ov.72h after CCl_4.

Ethanol feeding inhibits the recovery of cellular NAD+/NADH ratios after CCl_4 independent of Egr-1. Looking beyond Nqo1's ability to eliminate ROS and stabilize microtubules, it also plays a role in the modulation of reduced to oxidized nicotinamide nucleotide ratios. Not only does Nqo1 require FAD as a cofactor for its enzymatic activity, but it also contains a NAD(P)H binding site. During times of cell injury as in ethanol feeding or succeeding CCl_4 exposure, levels of NADH rise in the cell as NAD+ is used as a coenzyme in metabolism [38]. NADH can then bind Nqo1, donating an electron to FAD and allowing quinone substrates to bind the reduced FAD-enzyme complex for detoxification [39]. During this process, NADH is oxidized to NAD+, helping to restore the cellular redox state to a nicotinamide nucleotide ratio in favor of NAD+. Similar to results shown by Yuki et. al [38], CCl_4 significantly reduced cellular NAD+/NADH ratios 48h after treatment, favoring accumulation of NADH (Fig. 8). While there was partial recovery of NAD+ by 72h in pair-fed animals, ethanol feeding resulted in inhibition of reoxidation of NADH in both genotypes. However, since these ratios did not differ between genotypes, we concluded that inhibition of NADH reoxidation in Egr-1 deficient mice does not contribute to the enhanced fibrogenic changes seen in these animals following treatment with CCl_4.

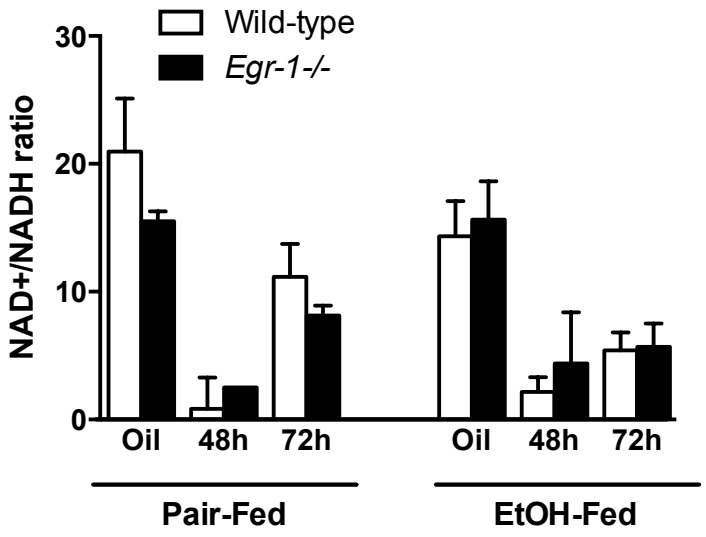

Figure 8. Ethanol feeding inhibits the recovery of cellular NAD+/NADH ratios after CCl_4 independent of Egr-1. NADH decreases during cell injury and is necessary for maintaining cell homeostasis. An NAD+/NADH quantification colorimetric assay was performed on wild-type and *Egr-1 -/-* livers 48 and 72h post CCl_4.

β-Lapachone-mediated increases in Nqo1 activity inhibit the induction of early markers of fibrosis in wild-type mice after CCl_4. β-Lapachone (βL), isolated from the bark of the lapacho tree, has been identified as a potent enzymatic activator of Nqo1 [40]. Recently, researchers have taken advantage of Nqo1 overexpression in some cancers, using Nqo1-mediated bioactivation of βL and other quinone-derived chemotherapeutic agents to exert cytotoxic effects on cells in cancer treatment [41]. Since increased NADH oxidation by βL has previously been shown to ameliorate metabolic syndrome and attenuate cisplatin-induced renal injury [42, 43], pharmacological activation of Nqo1 was used to better understand the importance of Nqo1 induction in the protection against fibrogenic changes in the liver after ethanol feeding and CCl_4 exposure. We administered βL to increase basal levels of Nqo1 activity in wild-type mice to attenuate the appearance

of early markers of hepatic fibrosis. Seventy-two hours after treatment with CCl_4, Nqo1 activity was increased (Fig. 9A), and CCl_4-induced elevation of plasma ALT activity was reduced in βL-treated animals compared to control (Fig. 9B). Additionally, HSC activation, as measured by Col1a1 and αSMA transcript levels, was decreased in βL-treated mice (Fig. 9C-D). These results suggest that stimulation of Nqo1 activity protects against CCl_4-induced liver injury.

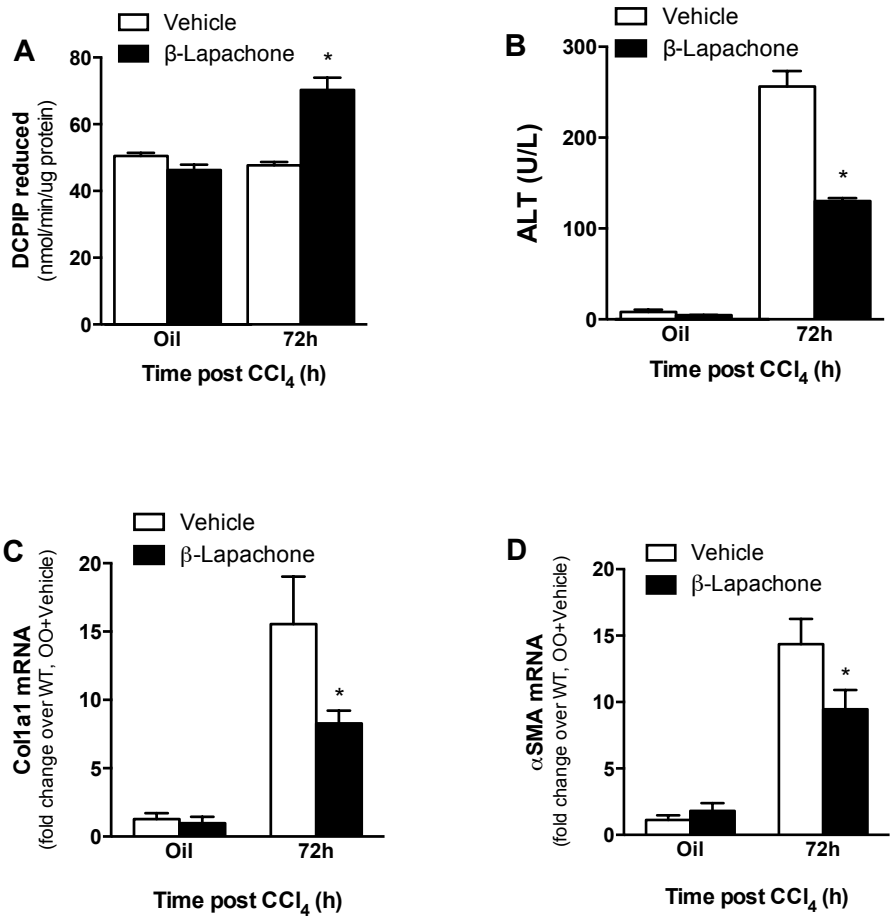

Figure 9. β-Lapachone-mediated induction of Nqo1 activity reduces the expression of early markers of fibrosis after CCl_4. (A) Nqo1 activity was assayed and reported as the amount of 2,6-dichlorophenolindophenol (DCPIP, substrate) reduced over time. (B) Plasma ALT activity was determined to assess liver injury 72h post CCl_4 in wild-type mice, while real-time PCR analysis was performed to measure quantities of (C) Col1a1 and (D) αSMA mRNA.

Discussion

Egr-1 has been extensively characterized in the regulation of genes critical to wound healing and is implicated in fibrosis [14]. While models of bleomycin-induced dermal and lung fibrosis exhibit attenuated disease in the absence of Egr-1 [15], models of cholestatic liver injury and hepatic fibrosis demonstrate increased injury with the loss of Egr-1 [17, 19]. Consistent with these studies in the liver, we demonstrated that Egr-1 deficiency protected against fibrogenic changes in the liver associated with moderate ethanol feeding and CCl_4 exposure, independent of changes in liver injury or CYP2E1-mediated bioactivation of CCl_4.

Multiple studies suggest that the oxidation of ethanol leads to an increase in Egr-1 expression [7, 44, 45]. Analogous to such studies in mice subjected to chronic ethanol feeding, peak induction of Egr-1 mRNA was enhanced in ethanol-fed mice compared to pair-fed mice 2h following CCl_4 administration (data not shown). This induction may be important for the initial inflammatory response following injury, but we suspect that the secondary induction in Egr-1 transcript levels seen in mice 48h post CCl_4 is more critical for the wound healing response accessory to inflammation, regulating extracellular matrix remodeling in a tightly controlled manner and reducing fibrosis. Therefore, the ethanol-dependent reduction in Egr-1 mRNA in mice at 48h may provide an additional explanation for the enhanced expression of early markers of fibrosis displayed in ethanol-fed animals in ours and other studies [20]. Interestingly, these same models have demonstrated that Egr-1 is required for the development of ethanol-induced steatosis through enhanced LPS sensitivity in Kuppfer cells and successive upregulation of TNFα [16]; however, we showed that the loss of Egr-1 delayed recovery of the liver from CCl_4-

induced steatosis, and ethanol feeding worsened this effect. While TNFα activation plays a role in the development of hepatic steatosis, there is considerable redundancy in the regulation of lipid metabolism, and so it is possible that the heightened steatosis in *Egr-1 -/-* mice seen 72h after CCl_4 is independent of TNFα expression.

The rapid and transient induction of Egr-1 by oxidative stress in the progression of a number of diseases led us to hypothesize that Egr-1 may regulate antioxidants crucial for the detoxification of CCl_4-induced liver injury. While research has shown that Egr-1-dependent gene expression of SOD1 appeared to play a role in the control of oxidant stress in atherosclerotic lesions [46], we found no change in expression of SOD 1 or 2 in *Egr-1 -/-* mice 72h after ethanol feeding and CCl_4. However, an oxidant stress, antioxidant defense pathway array and sequential analysis by real-time PCR and Western blot elucidated the antioxidant Nqo1 as a potential target of Egr-1 and mediator of cellular protection from oxidative damage. Expressed at low levels under basal conditions, Nqo1 induction is thought to be more important during periods of hepatic injury and oxidative stress [47]. For example, Nqo1 protein and activity was markedly elevated in mouse liver following bile duct ligation as well as following exposure to hepatoxicants such as acetaminophen (APAP) and CCl_4 [48]. Unexpectedly, despite increased levels of Nqo1 mRNA and protein, abrogated by Egr-1 deficiency and ethanol feeding, analysis of oxidative stress and cellular antioxidant capacity illustrated no differences between diets and genotypes after CCl_4 exposure. Surprisingly, although we demonstrated that the loss of Nqo1 via Egr-1 deficiency did not affect NADH reoxidation 72h after CCl_4, we showed that β-Lapachone administration attenuated liver injury and fibrogenic changes induced by CCl_4 through activation of Nqo1 activity. Together, these

data suggest that accumulation of NADH and loss of antioxidant defense does not contribute to enhanced fibrogenesis in Egr-1 deficient mice. However, the attenuation of liver injury by βL does not rule out a protective role for Nqo1 in hepatic fibrosis.

βL, a naturally occurring compound that has been used medicinally for years, has several known modes of action through which it can trigger apoptosis in Nqo1-overexpressing cancer cells. Originally discovered as an inhibitor of DNA topoisomerase I, βL toxicity is associated with single and double strand DNA breaks as well as inhibition of DNA replication [49]. Whereas quinone metabolism by Nqo1 normally produces stable hydroquinone species that are conjugated for excretion, metabolism of βL by Nqo1 generates a reactive, unstable hydroquinone that is oxidized to a semiquinone [50]. Semiquinones are free radicals that stimulate redox cycling and lead to production of ROS such as superoxide and hydrogen peroxide, which can damage the cell. Reduction of βL by Nqo1 additionally leads to futile cycling between its quinone and hydroquinone forms causing depletion of cytosolic NADH and subsequent activation of calpain-mediated cell death. While similar studies in which βL attenuated cisplatin-induced renal injury showed suppression of critical mediators of inflammation and ROS by NAD-dependent activation of Sirt1 [43], we showed that βL abated CCl_4-induced liver injury independent of increased intracellular NAD+. We demonstrated that treatment with βL did in fact enhance Nqo1 activity, and transcript levels of Col1a1 and αSMA, expressed by activated HSC, were decreased in βL-treated mice compared to vehicle treated mice. However, we suspect that the reduction in injury and markers of fibrogenesis is more likely due to the activation of apoptotic signaling pathways in hepatic stellate cells. While stellate cells may undergo senescence or revert back to a

quiescent phenotype after activation, apoptosis is also prominent in stellate cells and is an important mechanism for the regression of fibrosis [51]. Though previous studies have shown the stimulation of apoptosis in HSC to be an attractive anti-fibrotic therapeutic approach [52], further studies should be done to investigate the mechanisms by which βL inhibits CCl_4-induced liver injury.

Additionally, following these studies, RNA sequencing and validation with real-time PCR identified reduction in several carboxylesterase (*Ces*) 1 isoforms (Table 3, Fig. 10A), identifying an alternative method of lipogenic dysregulation after CCl_4, independent of NADH accumulation. Recent studies have reported that global *Ces1 -/-* mice develop hepatic steatosis and that activation of Ces1 in the liver lowered hepatic triglyceride levels and improved glucose tolerance in obese mice through previously unrecognized triglyceride hydrolase activity [53]. Reduced triglyceride hydrolase activity due to polymorphisms in other triglyceride lipases such as adipose triglyercide lipase (ATGL), patatin-like phospholipase domain-containing (PNPLA) 2 and 3 predisposes patients towards the full spectrum of liver damage associated with fatty liver [54, 55]. Consistently, we found complete inhibition of PNPLA3 mRNA in *Egr-1 -/-* mice compared to wild-type 48 and 72h after CCl_4 (Fig. 10B). This evidence of perturbed lipid homeostatic mechanisms provides an additional explanation for increased steatosis seen in ethanol-fed, CCl_4-exposed *Egr-1 -/-* mice. Furthermore, additional RNA sequencing data highlighted increases in profibrotic mediators as well as loss of glutathione-s-transfersases in these animals (Table 3). Collectively, these pathways strongly imply a protective role for Egr-1 in the development of hepatic fibrosis following ethanol-

accelerated, CCl_4-induced liver injury that would be of great interest to explore in future studies.

Although it has been reported that Egr-1 mRNA expression is heightened in livers of patients with chronic cholestasis [56], the status of Egr-1 in patients with ALD remains unclear. Not only would understanding the expression of Egr-1 in human fibrosis be essential, but further studies would also be required to understand the functions of other Egr-1-expressing cell types in the development of liver fibrosis. Consistent with CCl_4-mediated increases in Nqo1 mRNA and protein we saw in whole liver, initial studies in APAP-induced liver injury and primary biliary cirrhosis show that Nqo1 expression and activity are also increased in hepatocytes of these two types of human liver disease [47]. Interestingly, while we showed that expression of Nqo1 was increased by CCl_4 exposure in whole liver, which was reduced by Egr-1 deficiency and ethanol feeding, Nqo1 mRNA decreased during plate-induced activation of wild-type HSC and the loss of Egr-1 robustly enhanced this effect. We postulate that because Nqo1 is a negative regulator of fibrosis, its downregulation is critical for the activation of HSC in fibrogenesis. Therefore, it will be very important to investigate and consider Egr-1 function in the many cell types involved in the development of hepatic fibrosis for more directly targeted therapeutic treatments.

In future studies, we would like to corroborate our chromatin immunoprecipitation findings with a luciferase reporter assay and electrophoretic mobility shift assay. Comparative to pharmacological activation of Nqo1, we would also like to pharmacologically inhibit Nqo1 with dicoumarol or ES936 to establish that the attenuation of hepatic fibrosis by Egr-1 is Nqo1-dependent [36, 57]. Similarly, the use of

Nqo1 -/- mice could affirm this hypothesis. Importantly, in addition to the functions of Nqo1 that we have investigated throughout this study, Nqo1 also regulates protein degradation through interaction with the 20S proteasome [57]. Therefore, to understand the mechanisms by which Nqo1 contributes to protection from fibrosis, we will investigate how Nqo1's association with the 20S proteasome may be a contributing factor. Additionally, further validation of results obtained from RNA sequencing may elucidate other pathways essential to the attenuation of liver fibrosis by Egr-1. Futhermore, determining the function of other Egr-1-expressing cell types in liver disease progression as well as the status of Egr-1 in primary human hepatocytes of ALD patients will help us better understand the role of Egr-1 in human liver disease.

In summary, ethanol feeding reduces Egr-1 during fibrogenesis in response to CCl_4-induced liver injury in wild-type mice. Independent of enhanced peak liver injury and bioactivation of CCl_4, Egr-1 deficient mice had significantly increased levels of αSMA mRNA and protein as well as increased expression of type I collagen compared to wild-type mice. Ethanol feeding potentiated this effect. Of interest, the increase in early fibrosis markers in Egr-1 null mice was accompanied by an increase in hepatic triglycerides 72h after CCl_4 and by inhibition of Nqo1 induction, which was exacerbated by ethanol feeding. Chromatin immunoprecipitation confirmed direct binding of Egr-1 to the *Nqo1* promoter, introducing Nqo1 as a novel gene target of Egr-1. Although reduction of Nqo1 did not affect oxidative damage, mitotic spindle assembly, or NADH oxidation in *Egr-1 -/-* mice compared to wild-type, attenuation of CCl_4-mediated liver injury and fibrogenic changes by β-Lapachone suggests a potential role for Nqo1 in protection from hepatic fibrosis. However, a better understanding of the disparate contributions of Egr-1

in different models of fibrosis as well as the mechanisms by which Nqo1 exerts inhibitory effects on CCl_4-induced liver injury is crucial for development of therapeutic anti-fibrotic interventions targeting the two.

Table 3: Genes differentially regulated in *Egr-1 -/-* mice after CCl_4 exposure

FIBROSIS		ANTI-OXIDANT		LIPID HOMEOSTASIS	
GENE	**FOLD CHANGE**	**GENE**	**FOLD CHANGE**	**GENE**	**FOLD CHANGE**
Ctgf	3.8	*Gsta1*	-12.2	*Ces1b*	-11.1
Mmp9	3.7	*Gsta2*	-30.6	*Ces1d*	-28.08
Col2A1	4.1	*Nqo1*	-12.5	*Ces1e*	-8.8
Lox	3.3			*Ces2a*	-48.4

Table 3. A Next Gen Sequencing pilot project identified 3 interralated networks whose dysregulation is associated with an enhanced fibrogenic phenotype in ethanol-fed, Egr-1 deficient mice after CCl_4 exposure. Fold changes indicated show differences in expression between CCl_4-exposed, wild-type and *Egr-1 -/-* mice.

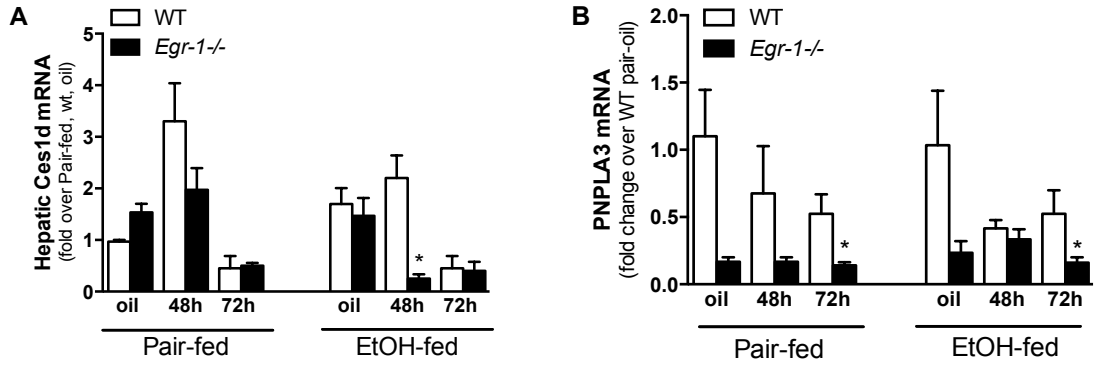

Figure 10. Egr-1 deficiency limits hepatic lipid-regulatory mRNA induction after CCl_4 exposure; ethanol-feeding further suppresses these genes. Hepatic accumulation of (A) Ces1d and (B) PNPLA3 transcripts was determined by real-time PCR 48 and 72h after CCl_4, validating RNAseq data.

References

1. Bouchery, E.E., et al., *Economic costs of excessive alcohol consumption in the U.S., 2006.* Am J Prev Med, 2011. **41**(5): p. 516-24.
2. Stahre, M., et al., *Contribution of excessive alcohol consumption to deaths and years of potential life lost in the United States.* Prev Chronic Dis, 2014. **11**: p. E109.
3. Lieber, C.S., *Alcoholic fatty liver: its pathogenesis and mechanism of progression to inflammation and fibrosis.* Alcohol, 2004. **34**(1): p. 9-19.
4. Liu, J., *Ethanol and liver: Recent insights into the mechanisms of ethanol-induced fatty liver.* World J Gastroenterol, 2014. **20**(40): p. 14672-14685.
5. Menon, K.V., G.J. Gores, and V.H. Shah, *Pathogenesis, diagnosis, and treatment of alcoholic liver disease.* Mayo Clin Proc, 2001. **76**(10): p. 1021-9.
6. Liu, J., et al., *Carvedilol attenuates the progression of alcohol fatty liver disease in rats.* Alcohol Clin Exp Res, 2012. **36**(9): p. 1587-99.
7. Pritchard, M.T. and L.E. Nagy, *Ethanol-induced liver injury: potential roles for egr-1.* Alcohol Clin Exp Res, 2005. **29**(11 Suppl): p. 146s-150s.
8. McMullen, M.R., et al., *Early growth response-1 transcription factor is essential for ethanol-induced fatty liver injury in mice.* Gastroenterology, 2005. **128**(7): p. 2066-76.
9. Sukhatme, V.P., et al., *A zinc finger-encoding gene coregulated with c-fos during growth and differentiation, and after cellular depolarization.* Cell, 1988. **53**(1): p. 37-43.
10. Zhang, Y., et al., *Diurnal regulation of the early growth response 1 (Egr-1) protein expression by hepatocyte nuclear factor 4alpha (HNF4alpha) and small heterodimer partner (SHP) cross-talk in liver fibrosis.* J Biol Chem, 2011. **286**(34): p. 29635-43.
11. Braddock, M., *The transcription factor Egr-1: a potential drug in wound healing and tissue repair.* Ann Med, 2001. **33**(5): p. 313-8.
12. Bhattacharyya, S., et al., *Smad-independent transforming growth factor-beta regulation of early growth response-1 and sustained expression in fibrosis: implications for scleroderma.* Am J Pathol, 2008. **173**(4): p. 1085-99.
13. Kim, N.D., et al., *Early growth response factor-1 is critical for cholestatic liver injury.* Toxicol Sci, 2006. **90**(2): p. 586-95.
14. Wu, M., et al., *Essential roles for early growth response transcription factor Egr-1 in tissue fibrosis and wound healing.* Am J Pathol, 2009. **175**(3): p. 1041-55.
15. Bhattacharyya, S., et al., *Early growth response transcription factors: key mediators of fibrosis and novel targets for anti-fibrotic therapy.* Matrix Biol, 2011. **30**(4): p. 235-42.
16. Pritchard, M.T., et al., *Early growth response-1 contributes to galactosamine/lipopolysaccharide-induced acute liver injury in mice.* Am J Physiol Gastrointest Liver Physiol, 2007. **293**(6): p. G1124-33.
17. Sullivan, B.P., et al., *Early growth response factor-1 limits biliary fibrosis in a model of xenobiotic-induced cholestasis in mice.* Toxicol Sci, 2012. **126**(1): p. 267-74.

18. Pritchard, M.T. and L.E. Nagy, *Hepatic fibrosis is enhanced and accompanied by robust oval cell activation after chronic carbon tetrachloride administration to Egr-1-deficient mice.* Am J Pathol, 2010. **176**(6): p. 2743-52.
19. Pritchard, M.T., et al., *Early growth response-1 attenuates liver injury and promotes hepatoprotection after carbon tetrachloride exposure in mice.* J Hepatol, 2010. **53**(4): p. 655-62.
20. Roychowdhury, S., et al., *Inhibition of apoptosis protects mice from ethanol-mediated acceleration of early markers of CCl4 -induced fibrosis but not steatosis or inflammation.* Alcohol Clin Exp Res, 2012. **36**(7): p. 1139-47.
21. Pritchard, M.T., R.N. Malinak, and L.E. Nagy, *Early growth response (EGR)-1 is required for timely cell-cycle entry and progression in hepatocytes after acute carbon tetrachloride exposure in mice.* Am J Physiol Gastrointest Liver Physiol, 2011. **300**(6): p. G1124-31.
22. Nasongkla, N., et al., *Enhancement of solubility and bioavailability of beta-lapachone using cyclodextrin inclusion complexes.* Pharm Res, 2003. **20**(10): p. 1626-33.
23. Nagy, L.E., *Alcohol: Methods and protocols.* . 2008, Totowa, NJ: Humana Press.
24. Wu, D. and A.I. Cederbaum, *Development and properties of HepG2 cells that constitutively express CYP2E1.* Methods Mol Biol, 2008. **447**: p. 137-50.
25. Moffit, J.S., et al., *Role of NAD(P)H:quinone oxidoreductase 1 in clofibrate-mediated hepatoprotection from acetaminophen.* Toxicology, 2007. **230**(2-3): p. 197-206.
26. Hughes, H., H. Jaeschke, and J.R. Mitchell, *Measurement of oxidant stress in vivo.* Methods Enzymol, 1990. **186**: p. 681-5.
27. Schneider, C.A., W.S. Rasband, and K.W. Eliceiri, *NIH Image to ImageJ: 25 years of image analysis.* Nat Methods, 2012. **9**(7): p. 671-5.
28. Pagel, J.I. and E. Deindl, *Disease progression mediated by egr-1 associated signaling in response to oxidative stress.* Int J Mol Sci, 2012. **13**(10): p. 13104-17.
29. Koop, D.R., *Alcohol metabolism's damaging effects on the cell: a focus on reactive oxygen generation by the enzyme cytochrome P450 2E1.* Alcohol Res Health, 2006. **29**(4): p. 274-80.
30. Kubosaki, A., et al., *Genome-wide investigation of in vivo EGR-1 binding sites in monocytic differentiation.* Genome Biol, 2009. **10**(4): p. R41.
31. Friedman, S.L., *Molecular regulation of hepatic fibrosis, an integrated cellular response to tissue injury.* J Biol Chem, 2000. **275**(4): p. 2247-50.
32. Siegel, D., et al., *NAD(P)H:quinone oxidoreductase 1: role as a superoxide scavenger.* Mol Pharmacol, 2004. **65**(5): p. 1238-47.
33. Weber, L.W., M. Boll, and A. Stampfl, *Hepatotoxicity and mechanism of action of haloalkanes: carbon tetrachloride as a toxicological model.* Crit Rev Toxicol, 2003. **33**(2): p. 105-36.
34. Cabre, M., et al., *Time-course of changes in hepatic lipid peroxidation and glutathione metabolism in rats with carbon tetrachloride-induced cirrhosis.* Clin Exp Pharmacol Physiol, 2000. **27**(9): p. 694-9.
35. Wignall, S.M., et al., *Identification of a novel protein regulating microtubule stability through a chemical approach.* Chem Biol, 2004. **11**(1): p. 135-46.

36. Siegel, D., J.K. Kepa, and D. Ross, *NAD(P)H:quinone oxidoreductase 1 (NQO1) localizes to the mitotic spindle in human cells.* PLoS One, 2012. **7**(9): p. e44861.
37. Liao, Y., et al., *Delayed hepatocellular mitotic progression and impaired liver regeneration in early growth response-1-deficient mice.* J Biol Chem, 2004. **279**(41): p. 43107-16.
38. Yuki, T., et al., *Alteration of hepatic ethanol metabolism in CCL4-intoxicated rats: analysis using isolated liver perfusion system.* Subst Alcohol Actions Misuse, 1982. **3**(3): p. 163-75.
39. Asher, G., et al., *The crystal structure of NAD(P)H quinone oxidoreductase 1 in complex with its potent inhibitor dicoumarol.* Biochemistry, 2006. **45**(20): p. 6372-8.
40. Planchon, S.M., et al., *Beta-lapachone-mediated apoptosis in human promyelocytic leukemia (HL-60) and human prostate cancer cells: a p53-independent response.* Cancer Res, 1995. **55**(17): p. 3706-11.
41. Pardee, A.B., Y.Z. Li, and C.J. Li, *Cancer therapy with beta-lapachone.* Curr Cancer Drug Targets, 2002. **2**(3): p. 227-42.
42. Hwang, J.H., et al., *Pharmacological stimulation of NADH oxidation ameliorates obesity and related phenotypes in mice.* Diabetes, 2009. **58**(4): p. 965-74.
43. Oh, G.S., et al., *Pharmacological activation of NQO1 increases NAD(+) levels and attenuates cisplatin-mediated acute kidney injury in mice.* Kidney Int, 2014. **85**(3): p. 547-60.
44. Thomes, P.G., et al., *Cellular steatosis in ethanol oxidizing-HepG2 cells is partially controlled by the transcription factor, early growth response-1.* Int J Biochem Cell Biol, 2013. **45**(2): p. 454-63.
45. Donohue, T.M., Jr., et al., *Early growth response-1 contributes to steatosis development after acute ethanol administration.* Alcohol Clin Exp Res, 2012. **36**(5): p. 759-67.
46. McCaffrey, T.A., et al., *High-level expression of Egr-1 and Egr-1-inducible genes in mouse and human atherosclerosis.* J Clin Invest, 2000. **105**(5): p. 653-62.
47. Aleksunes, L.M., M. Goedken, and J.E. Manautou, *Up-regulation of NAD(P)H quinone oxidoreductase 1 during human liver injury.* World J Gastroenterol, 2006. **12**(12): p. 1937-40.
48. Aleksunes, L.M., et al., *Differential expression of mouse hepatic transporter genes in response to acetaminophen and carbon tetrachloride.* Toxicol Sci, 2005. **83**(1): p. 44-52.
49. Pink, J.J., et al., *NAD(P)H:Quinone oxidoreductase activity is the principal determinant of beta-lapachone cytotoxicity.* J Biol Chem, 2000. **275**(8): p. 5416-24.
50. Park, E.J., et al., *beta-Lapachone induces programmed necrosis through the RIP1-PARP-AIF-dependent pathway in human hepatocellular carcinoma SK-Hep1 cells.* Cell Death Dis, 2014. **5**: p. e1230.
51. Rockey, D.C., *Translating an understanding of the pathogenesis of hepatic fibrosis to novel therapies.* Clin Gastroenterol Hepatol, 2013. **11**(3): p. 224-31.e1-5.

52. Wright, M.C., et al., *Gliotoxin stimulates the apoptosis of human and rat hepatic stellate cells and enhances the resolution of liver fibrosis in rats.* Gastroenterology, 2001. **121**(3): p. 685-98.
53. Xu, J., et al., *Hepatic carboxylesterase 1 is essential for both normal and farnesoid X receptor-controlled lipid homeostasis.* Hepatology, 2014. **59**(5): p. 1761-71.
54. Steinberg, G.R., B.E. Kemp, and M.J. Watt, *Adipocyte triglyceride lipase expression in human obesity.* Am J Physiol Endocrinol Metab, 2007. **293**(4): p. E958-64.
55. Dongiovanni, P., et al., *PNPLA3 I148M polymorphism and progressive liver disease.* World J Gastroenterol, 2013. **19**(41): p. 6969-78.
56. Allen, K., et al., *Upregulation of early growth response factor-1 by bile acids requires mitogen-activated protein kinase signaling.* Toxicol Appl Pharmacol, 2010. **243**(1): p. 63-7.
57. Adamovich, Y., et al., *The protein level of PGC-1alpha, a key metabolic regulator, is controlled by NADH-NQO1.* Mol Cell Biol, 2013. **33**(13): p. 2603-13.